

## PTEN Is a Potent Suppressor of Small Cell Lung Cancer

Min Cui<sup>1</sup>, Arnaud Augert<sup>2</sup>, Michael Rongione<sup>1</sup>, Karina Conkrite<sup>1</sup>, Susan Parazzoli<sup>2</sup>, Alexander Yu. Nikitin<sup>3</sup>, Nicholas Ingolia<sup>1</sup>, and David MacPherson<sup>1,2</sup>

### Abstract

Small cell lung carcinoma (SCLC) is a highly metastatic tumor type with neuroendocrine features and a dismal prognosis. *PTEN* mutations and *PIK3CA* activating mutations have been reported in SCLC but the functional relevance of this pathway is unknown. The *PTEN/PIK3CA* pathway was interrogated using an AdenoCre-driven mouse model of SCLC harboring inactivated *Rb* and *p53*. Inactivation of one allele of *PTEN* in *Rb/p53*-deleted mice led to accelerated SCLC with frequent metastasis to the liver. In contrast with the high mutation burden reported in human SCLC, exome analyses revealed a low number of protein-altering mutations in mouse SCLC. Inactivation of both alleles of *PTEN* in the *Rb/p53*-deleted system led to nonmetastatic adenocarcinoma with neuroendocrine differentiation. This study reveals a critical role for the PTEN/PI3K pathway in both SCLC and lung adenocarcinoma and provides an ideal system to test the phosphoinositide 3-kinase (PI3K) pathway inhibitors as targeted therapy for subsets of patients with SCLC.

**Implications:** The ability of *PTEN* inactivation to accelerate SCLC in a genetic mouse model suggests that targeting the *PTEN* pathway is a therapeutic option for a subset of human patients with SCLC.

**Visual Overview:** <http://mcr.aacrjournals.org/content/early/2014/04/28/1541-7786.MCR-13-0554/F1.large.jpg>. *Mol Cancer Res*; 12(5); 654–9. ©2014 AACR.

### Introduction

Small cell lung carcinoma (SCLC) is a highly metastatic neuroendocrine tumor that results in the deaths of >20,000 people per year in the United States alone. It has been known that the *p53* and *RB* tumor suppressor genes are mutated in the majority of SCLCs, and that *MYC* family members are frequently amplified (1, 2). Alterations in the *PTEN* pathway have also been reported in SCLC, through direct *PTEN* mutation/deletion (3, 4) or through *PIK3CA* activation (5). *PIK3CA* and/or *PTEN* mutations were more recently found in two recent next-generation sequencing studies of SCLC (6, 7). The huge number of somatic mutations in human SCLC (6–8) necessitates the functional evaluation of key SCLC-mutated genes. As inhibition of phosphoinositide

3-kinase (PI3K) or the downstream effectors AKT and mTOR can be achieved using targeted therapies, the importance of the PTEN pathway in SCLC is particularly critical to elucidate. Murine models for SCLC have been generated that accurately recapitulate the cardinal features of human SCLC, including recapitulating key secondary alterations (9–12). In this study, we use a mouse model to interrogate *PTEN* as a potential SCLC driver.

### Materials and Methods

#### Mice

*Rb<sup>lox</sup>* mice were obtained from Tyler Jacks (MIT). *p53<sup>lox</sup>* mice were generated by Anton Berns (Netherlands Cancer Institute; Amsterdam, the Netherlands) and obtained from the Mouse Models of Human Cancer Consortium. *Pten<sup>lox</sup>* mice were generated by Hong Wu (University of California, Los Angeles; Los Angeles, CA) and obtained from Jackson Laboratories. All mice were maintained on a mixed genetic background. Mouse experiments were approved by the Animal Use and Care Committees at the Carnegie Institution (Baltimore, MD) and Fred Hutchinson Cancer Research Center (Seattle, WA).

**AdenoCre SCLC mode.** After breeding the *Pten<sup>lox</sup>* allele into the *Rb<sup>lox/lox</sup>p53<sup>lox/lox</sup>* background, *Rb<sup>lox/lox</sup>; p53<sup>lox/lox</sup>; Pten<sup>lox/+</sup>* mice were intercrossed to obtain littermate controls that differed in *Pten* status. Mice were infected with  $1 \times 10^8$

**Authors' Affiliations:** <sup>1</sup>Department of Embryology, Carnegie Institution, Baltimore, Maryland; <sup>2</sup>Fred Hutchinson Cancer Research Center, Seattle, Washington; and <sup>3</sup>Department of Biomedical Sciences, Cornell University, Ithaca, New York

**Note:** Supplementary data for this article are available at Molecular Cancer Research Online (<http://mcr.aacrjournals.org/>).

**Corresponding Author:** David MacPherson, Division of Human Biology, Fred Hutchinson Cancer Research Center, 1100 Fairview Avenue North, Seattle, WA 98109. Phone: 206-667-6464; Fax: 206-667-2917; E-mail: dmacpher@fhcrc.org

doi: 10.1158/1541-7786.MCR-13-0554

©2014 American Association for Cancer Research.

pfu AdenoCre driven by the cytomegalovirus promoter (University of Iowa Gene Transfer Core; Iowa City, IA) in 75  $\mu$ L using intratracheal intubation as described (13). Mice were aged until moribund and the lungs were fixed in 4% paraformaldehyde or Bouin solution for histologic analyses. The following antibodies were used for immunohistochemistry: calcitonin gene-related peptide (CGRP; 1/2,000, Sigma), synaptophysin (1/33, Invitrogen), and CK19 (1/250, Abcam ab52625). CGRP immunostaining was performed on Bouin fixed tissue. Antigen retrieval was performed using boiling sodium citrate (pH 6.0) and samples were incubated overnight with primary antibody. We used the Vectastain ABC Kit (Vector Laboratories) for biotin-mediated signal amplification, and horseradish peroxidase-based detection was with 3, 3'-diaminobenzidine (Vector Laboratories).

**Real-time PCR.** Total RNA from lung tumors was extracted using TRIzol reagent (Life Technologies). cDNAs were generated using random hexamer priming and Superscript III reverse transcriptase (Life Technologies). Real-time PCR was performed with Sybr Select master mix (Life Technologies) in 384-well format using an ABI 7900HT Real-Time PCR System. *Pten* copy number was examined by designing primers to exon 5 of the murine *Pten* gene and comparing  $C_t$  values relative to a control gene, *Actb* across phenol-chloroform isolated genomic DNA from tumors. All primer sequences used for real-time PCR are shown in Supplementary Table S1.

**Next-generation sequencing to identify SCLC mutations.** Mouse tumor or tail DNA was isolated following proteinase K digest and phenol-chloroform extraction. The SureSelectXT Mouse All Exon platform (Agilent Technologies) was used for exon capture and library preparation. Samples were sequenced using an Illumina HiSeq2000 with generation of 75bp paired end reads. The Burrows Wheeler Aligner (14) was used to align reads to the mouse mm9 reference genome. SAMtools was used to remove duplicates arising from PCR and was also used to detect variants (mismatches, and small insertions and deletions; ref. 15). Variant positions were identified from matched pairs of tumor samples and normal tissue or cell line controls using SAMtools with computation of genotype likelihood in each sample (options -u, -D, and -S). Variant genotypes were called using bcftools (15) with Bayesian inference, per-sample genotype calling, and contrast calling to determine the likelihood of different allele frequencies between the tumor and control samples (options -c, -g, and -1). Tumor-specific mutations were identified by filtering variants with probability of allele frequency difference between matched normal and tumor samples of  $P < 1e-10$  (i.e., PC2 > 100). Annovar was used to annotate variants (16). Protein altering mutations identified in exome analyses included nonsynonymous exonic mutations as well as intronic mutations in essential splice sites that were present in the tumor but not matched normal. Exome data coverage is shown in Supplementary Table S2.

**Western blotting.** Cell lysates were prepared in ice-cold radioimmunoprecipitation assay buffer (50 mmol/L Tris-HCl, pH 8.0, 150 mmol/L NaCl, 0.1% SDS, 1% NP-40,

and 0.5% sodium deoxycholate) supplemented with protease inhibitor tablets (Roche). The following primary antibodies were used: anti-PTEN (#9559, Cell Signaling Technology), anti-phospho Akt (Ser-473; #4060, Cell Signaling Technology), anti-Akt (#4691, Cell Signaling Technology) and anti-actin (sc-1615, Santa Cruz Biotechnology).

## Results

Despite previous reports of *PTEN* deletions (3, 4, 17) and *PIK3CA* activating mutations (5) in SCLC, the overall importance of the *PTEN/PIK3CA* pathway for this cancer remains unclear. Tumor dependence on mutations in the PTEN/PI3K pathway may provide an avenue for SCLC treatment through therapies that target this pathway. Thus, we explored the functional importance of this pathway for SCLC. To assess the importance of the PTEN/PI3K pathway for SCLC, we used the Berns SCLC mouse model (9). This model uses Adenoviral Cre (AdCre) to drive *Rb* and *p53* deletion. Resulting lung tumors arise with long latency and mimic critical features of human SCLC, including neuroendocrine characteristics and metastatic spread (9). We infected  $Rb^{lox/lox};p53^{lox/lox};Pten^{+/+}$ ,  $Rb^{lox/lox};p53^{lox/lox};Pten^{lox/+}$  and  $Rb^{lox/lox};p53^{lox/lox};Pten^{lox/lox}$  cohorts with AdCre delivered using intratracheal intubation. Cohorts were aged and followed until the mice were moribund.

### Hemizygous inactivation of *Pten* accelerates murine SCLC

Inactivation of *Rb/p53* led to morbidity from lung tumors arising with long latency. Mice in the *Rb/p53* cohort became moribund with lung tumor burden at an average  $\pm$  SD of  $387 \pm 57$  days (Fig. 1A). Tumors in the model were overall histologically similar to the SCLC tumors previously described (9). Most tumors exhibited neuroendocrine features, staining positively for neuroendocrine markers CGRP (Fig. 1B, inset) and synaptophysin (Supplementary Fig. S1), although variability in staining was observed. The SCLCs were aggressive with invasion into vessels and local lymph nodes (Fig. 1B and Supplementary Fig. S1). We noted a minor component of acinar adenocarcinoma with neuroendocrine differentiation in some *Rb/p53*-deficient tumors (Supplementary Fig. S1). Inactivation of one allele of *Pten* in the  $Rb^{lox/lox};p53^{lox/lox}$  background significantly accelerated tumorigenesis. Here, mice became moribund at an average  $\pm$  SD of  $242 \pm 59$  days (Fig. 1A) and lung tumors exhibited histologic features similar to the  $Rb^{lox/lox};p53^{lox/lox}$  model (Fig. 1C and Supplementary Fig. S2). Heterogeneity in CGRP and synaptophysin staining was seen within and between tumors in the  $Rb^{lox/lox};p53^{lox/lox};Pten^{lox/+}$  group. As in the  $Rb^{lox/lox};p53^{lox/lox}$  model, the major tumor component of the  $Rb^{lox/lox};p53^{lox/lox};Pten^{lox/+}$  mice was SCLC, with a minor component of adenocarcinoma. PCR analysis showed that both floxed alleles of *Rb* and *p53* were recombined in six of six  $Rb^{lox/lox};p53^{lox/lox};Pten^{lox/+}$  SCLCs examined (Supplementary Fig. S3A and S3B), and real-time PCR analysis of *Pten* copy number was consistent with loss of *Pten* heterozygosity in each case (Supplementary Fig. S3C). Necropsy

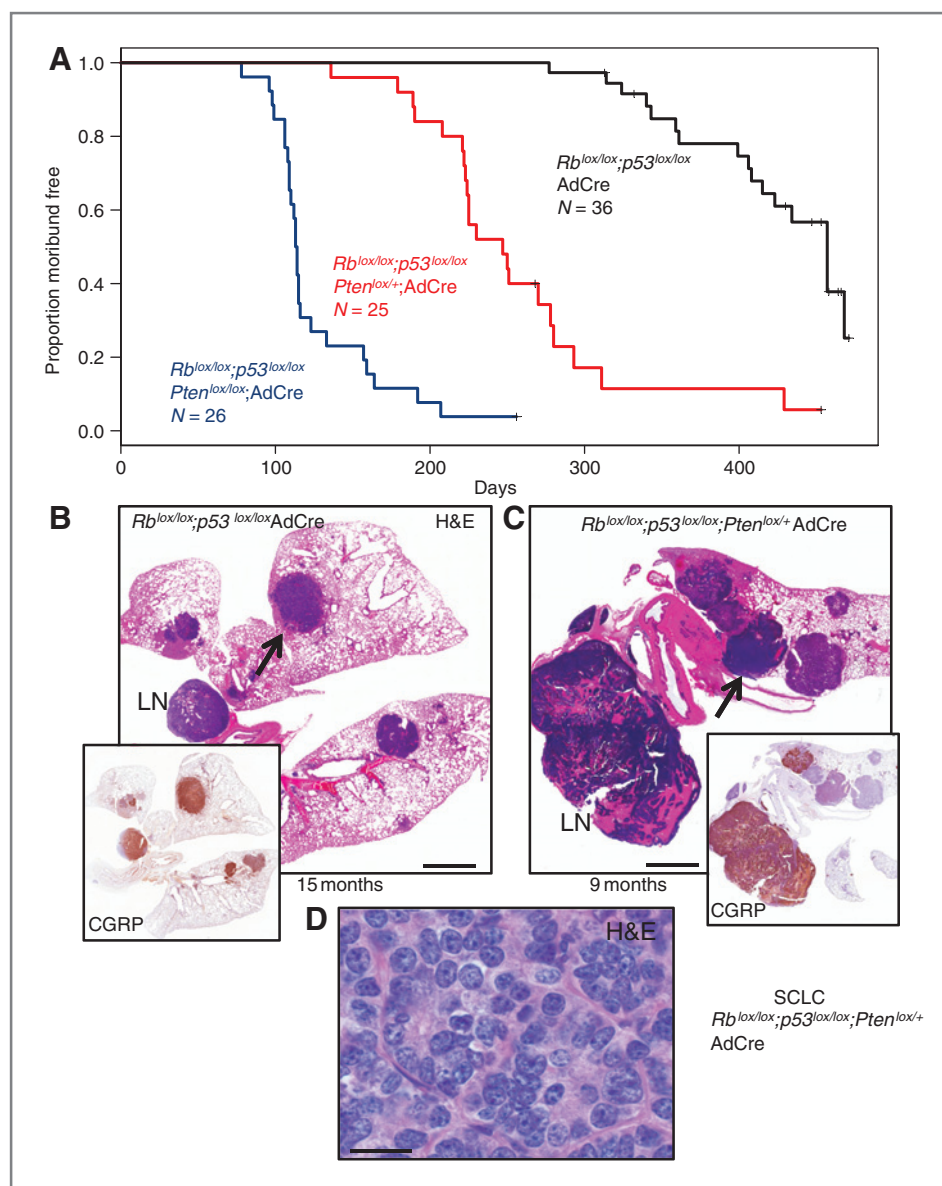


**Figure 1.** Inactivation of *Pten* accelerates *Rb/p53*-mutant lung tumors. A, Kaplan–Meier curves showing time to morbidity following AdCre delivery to *Rb<sup>lox/lox</sup>/p53<sup>lox/lox</sup>*, *Rb<sup>lox/lox</sup>;p53<sup>lox/lox</sup>/lox*, *Pten<sup>lox/+</sup>* and *Rb<sup>lox/lox</sup>;p53<sup>lox/lox</sup>;Pten<sup>lox/lox</sup>* mice. B, hematoxylin and eosin (H&E) stain of murine SCLC (arrow) from AdCre *Rb<sup>lox/lox</sup>;p53<sup>lox/lox</sup>* mouse at 15 months after AdCre with inset showing immunostaining for the neuroendocrine marker CGRP. Lymph node metastasis is indicated (LN). C, H&E of advanced SCLC in lymph node and lung (arrow) with CGRP immunostaining (inset) of *Rb<sup>lox/lox</sup>;p53<sup>lox/lox</sup>;Pten<sup>lox/+</sup>* lung at 9 months after AdCre. Heterogeneity in CGRP staining across tumor nodules is apparent. D, high magnification ( $\times 100$ ) image of H&E-stained SCLC from *Rb<sup>lox/lox</sup>;p53<sup>lox/lox</sup>;Pten<sup>lox/+</sup>* model. Scale bar for A, 2 mm; D, 13 microns.

analysis revealed gross liver metastasis in 16 of 25 of mice examined (64%) and histologic analyses of liver metastases showed exclusively SCLC. The strong acceleration of SCLC in a *Pten* heterozygous background reveals that *Pten* is a critical cooperating tumor suppressor gene in SCLC.

#### Homozygous inactivation of *Pten*

Adenoviral Cre delivered to *Rb<sup>lox/lox</sup>;p53<sup>lox/lox</sup>;Pten<sup>lox/lox</sup>* animals resulted in a distinct phenotype. Here, lung tumors arose extremely rapidly (average  $\pm$  SD of  $123 \pm 30$  days; Fig. 1A) with each lobe of the lung filled with tumors at the time of morbidity (Fig. 2A). The major component of the *Rb<sup>lox/lox</sup>;p53<sup>lox/lox</sup>;Pten<sup>lox/lox</sup>* tumors was acinar and mixed adenocarcinoma with neuroendocrine differentiation revealed by CGRP and synaptophysin immunohistochemistry (Fig. 2A–C). The tumors had acinar and papillary

patterns of growth (Fig. 2B). We also observed dysplastic and hyperplastic neuroendocrine lesions in the airways (Fig. 2D), likely precursor lesions to SCLC. The adenocarcinomas, including those with neuroendocrine features, stained positively for cytokeratin 19 (CK19; Fig. 2C), whereas the hyperplastic neuroendocrine lesions along the airways were negative for this marker (Fig. 2D). We note that SCLC tumors that arose in the *Rb<sup>lox/lox</sup>;p53<sup>lox/lox</sup>;Pten<sup>lox/+</sup>* model did not stain positively for CK19 (Supplementary Fig. S2). Also, although *Krt7* and *Krt18* mRNA expression was not significantly different between lung tumors in the *Rb<sup>lox/lox</sup>;p53<sup>lox/lox</sup>;Pten<sup>lox/lox</sup>* versus *Rb<sup>lox/lox</sup>;p53<sup>lox/lox</sup>;Pten<sup>lox/+</sup>* models, *Krt19* levels were significantly increased in the *Rb<sup>lox/lox</sup>;p53<sup>lox/lox</sup>;Pten<sup>lox/lox</sup>* adenocarcinoma model (Supplementary Fig. S4). Thus, despite common expression of neuroendocrine markers, the *Rb<sup>lox/lox</sup>*;

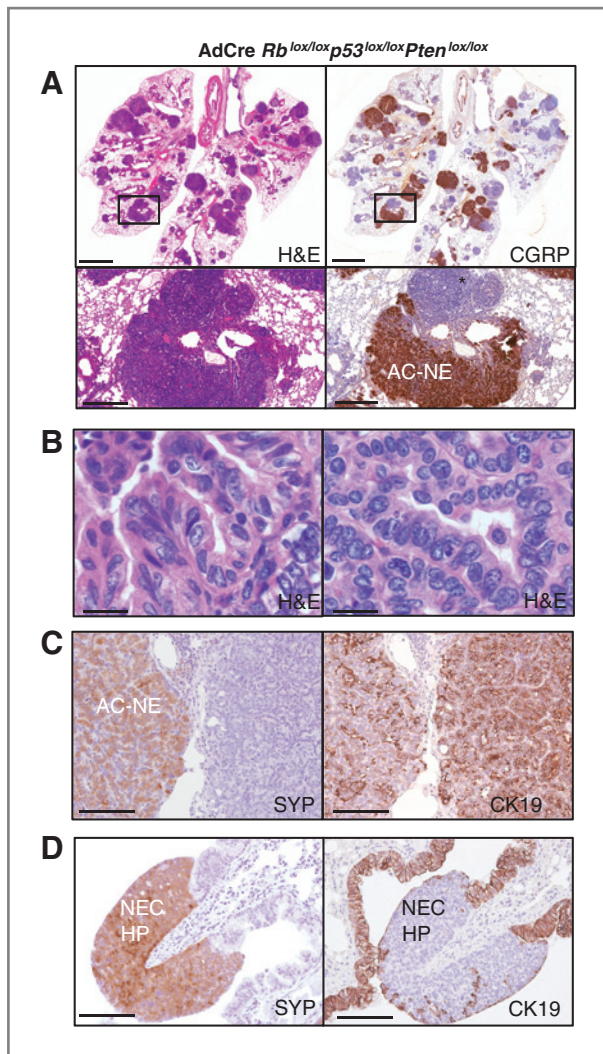


**Figure 2.** Homozygous *Pten* inactivation in *Rb/p53*-mutant lung. A, hematoxylin and eosin (H&E) stain showing tumor-filled lung from *Rb<sup>lox/lox</sup>; p53<sup>lox/lox</sup>; Pten<sup>lox/lox</sup>* mouse 3 months 20 days after AdCre (left). CGRP immunostaining of adjacent section showing neuroendocrine character of many tumor nodules (right). Boxed region shows magnified view of adenocarcinoma with neuroendocrine differentiation (Ac-NE) along with adenocarcinoma negative for CGRP (\*). B, high-magnification ( $\times 100$ ) view of adenocarcinoma histology. C, synaptophysin (SYP) and CK19 immunostaining of adenocarcinoma. Adjacent lesions both exhibit CK19 positivity, but only tumor area to left is synaptophysin positive. D, synaptophysin (SYP) positivity and absence of CK19 immunostaining in hyperplastic neuroendocrine cells along the airway (NEC-HP). Scale bars for A (top), 2 mm; A (bottom), 400 microns; B, 13 microns; C and D, 80 microns.

*p53<sup>lox/lox</sup>; Pten<sup>lox/+</sup>* SCLC and *Rb<sup>lox/lox</sup>; p53<sup>lox/lox</sup>; Pten<sup>lox/lox</sup>* adenocarcinoma models could be distinguished by histologic features and by CK19/Krt19 positivity. In contrast with the *Rb/p53* and *Rb/p53/Pten* heterozygous models, liver metastasis was not found in the *Pten* homozygote AdCre model. We did not perform long-term aging studies on *Pten<sup>lox/lox</sup>* mice in the context of wild-type *Rb* and *p53*. However, sacrifice of 5 nonmoribund *Pten<sup>lox/lox</sup>* animals

(wild-type for *Rb* and *p53*) at 5-months after AdCre did not reveal evidence of lung neoplasia (data not shown). Overall, these data indicate that homozygous *Pten* inactivation synergizes with *Rb* and *p53* loss to promote lung adenocarcinomas with neuroendocrine differentiation. The rapid lethality from many independent adenocarcinomas likely impaired development of advanced SCLC with liver metastasis in the *Pten* homozygous model.

### Molecular analyses of lung tumors

Western blot analysis of SCLCs from the *Pten* heterozygous model revealed complete loss of PTEN protein in four of four tumors examined (Fig. 3A). This is consistent with inactivation of the remaining wild-type *Pten* allele (Supplementary Fig. S3C). We were unable to control for the normal level of phospho-AKT in pulmonary

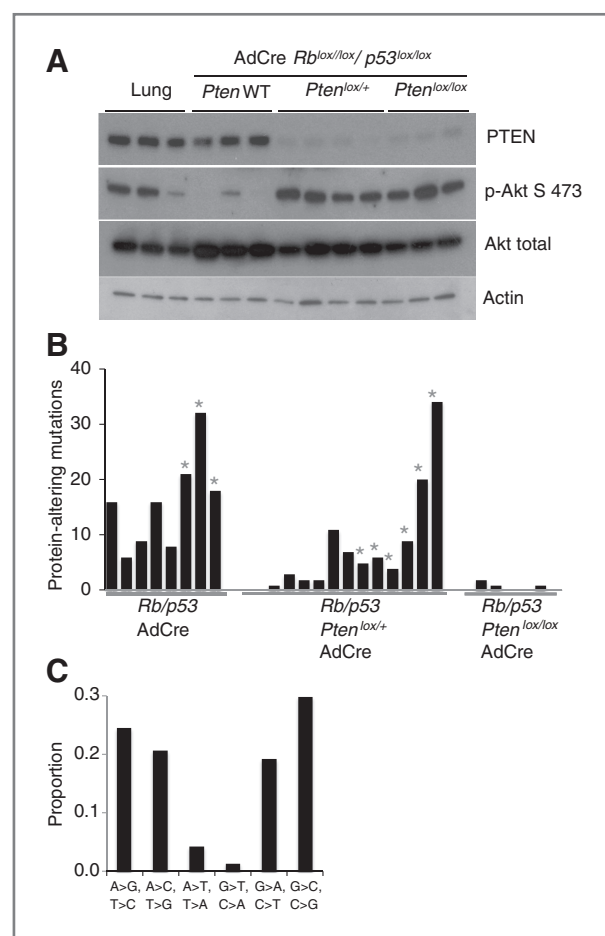


**Figure 3.** Analyses of murine lung neuroendocrine tumors. A, Western blot analyses of normal lung and SCLCs from the indicated genotypes showing PTEN, Phospho Akt S473, pan-AKT, and actin loading control. B, number of protein-altering mutations in murine lung neuroendocrine tumors of the indicated genotypes. Metastatic samples are indicated (\*). *Rb<sup>lox/lox</sup>; p53<sup>lox/lox</sup>*; eight tumors from 3 animals, *Rb<sup>lox/lox</sup>; p53<sup>lox/lox</sup>; Pten<sup>lox/+</sup>*; 13 tumors from 6 animals, *Rb<sup>lox/lox</sup>; p53<sup>lox/lox</sup>; Pten<sup>lox/lox</sup>*; six tumors from 3 animals. C, patterns of transitions and transversions in primary murine SCLC.

neuroendocrine cells in these Western blot analyses, as such cells are extremely rare in the lung. However, compared with *Pten* wild-type mouse SCLC, *Pten* hemizygous and homozygous lung tumors showed increased phosphorylation of AKT at Ser 473, indicative of pathway activation (Fig. 3A).

### Secondary alterations in lung tumors

Human SCLC is a smoking-associated cancer with high mutational load (6–8). In one study, an average of 175 protein-altering mutations per SCLC tumor were reported (7). To compare the somatic mutational load in murine SCLC with human SCLC, we performed whole-exome studies. In contrast with human SCLCs, the murine SCLC exome showed few protein-altering somatic mutations. We found an average of 15.8 protein altering mutations per murine SCLC in the *Rb<sup>lox/lox</sup>;p53<sup>lox/lox</sup>* model (Fig. 3B). *Pten* heterozygote tumors exhibited a variable and intermediate number of mutations (average 8 protein-altering mutations). There were no recurrent mutations or mutations in known cancer genes in this small sample set. We also characterized exonic mutations in the *Rb<sup>lox/lox</sup>;p53<sup>lox/lox</sup>;Pten<sup>lox/lox</sup>* lung adenocarcinomas; here, we found a near absence of selection for protein-altering mutations (average 0.7 mutations/tumor exome). In our murine exome analyses, on average, 92% of the mouse tumor exome was sequenced to 10× coverage whereas 82% was sequenced to 20× coverage (Supplementary Table S2). In contrast with human smoking-associated SCLC (6–8), C:G>A:T transversions in murine SCLC were infrequent (Fig. 3C). Thus, murine SCLC does not exhibit high numbers of point mutations typical of human smoking-associated SCLC.

### Discussion

*PTEN/PIK3CA* mutations have been described in SCLC; however, the overall importance of this pathway for SCLC is not clear. Thus, we tested the importance of this pathway using mouse genetics. We inactivated *Pten* in an *Rb/p53*-deleted mouse model of SCLC that recapitulates human SCLC in metastatic pattern and in neuroendocrine features (9). When even a single allele of *Pten* was inactivated, SCLC occurred with much faster kinetics. Moreover, the tumors in the *Pten* heterozygous model metastasized to the liver.

These data definitively show that *Pten* is a critical tumor suppressor in a genetic mouse model of SCLC. As there are no targeted therapies for SCLC, these data may provide incentive to treat human patients with SCLC with PI3K or Akt inhibitors. Murine SCLC models will be ideal for assessing the therapeutic potential of this approach.

Inactivation of both *Pten* alleles in the *Rb/p53* floxed background led to a shift in tumor spectrum. Multifocal adenocarcinomas, with the major component exhibiting neuroendocrine differentiation, led to rapid lethality. Interestingly, a subset of human adenocarcinomas that acquired resistance to targeted therapy acquired neuroendocrine characteristics and transformed into SCLC (18). In one patient, transformation to SCLC was associated with a newly

acquired activating PI3K mutation present in the SCLC but not in the original adenocarcinoma (18). It will be interesting to investigate whether the *RB*, *p53*, and/or *PTEN* pathway alteration can be linked to the acquisition of neuroendocrine properties in a non-neuroendocrine cell of origin. Application of neuroendocrine promoter-driven adenoviral vectors specifically to the lung (19) will enable late-stage SCLC modeling with homozygous *Pten* inactivation.

We found that murine SCLCs exhibited a lower number of protein-altering mutations than human SCLCs. In the AdCre *Rb<sup>lox/lox</sup>;p53<sup>lox/lox</sup>* model, we found 15.8 protein-altering mutations per tumor, a number much reduced in comparison with human SCLC. This difference is at least, in part, due to the fact that human SCLC typically arises in heavy smokers, leading to a high smoking-induced mutational burden. Hemizygoty for *Pten* in this model led to reduced somatic point mutations. The *Pten* hemizygous model will be particularly useful for studies of metastasis, as metastatic SCLC arises frequently and rapidly. Matched comparisons between primary and metastatic murine SCLCs may shed light on the genetic determinants of metastasis. The lower number of mutations in mouse SCLC models may facilitate study of individual SCLC-mutated genes. The high mutational burden in human SCLC is likely to lead to increased noise in similar analyses of human SCLC. Assessment of vulnerabilities to therapies associated with a specific mutation will be particularly informative using murine SCLC models given the reduced mutational complexity.

We demonstrated the critical role for the PTEN/PI3K pathway in SCLC. This finding has important implications for using targeted therapies directed toward this pathway to treat the most aggressive form of lung cancer.

### Disclosure of Potential Conflicts of Interest

No potential conflicts of interest were disclosed.

### Authors' Contributions

**Conception and design:** A. Augert, D. MacPherson

**Development of methodology:** M. Cui, K. Conkrite

**Acquisition of data (provided animals, acquired and managed patients, provided facilities, etc.):** M. Cui, M. Rongione, K. Conkrite, D. MacPherson

**Analysis and interpretation of data (e.g., statistical analysis, biostatistics, computational analysis):** M. Cui, A. Augert, A.Y. Nikitin, N. Ingolia, D. MacPherson

**Writing, review, and/or revision of the manuscript:** M. Cui, A. Augert, M. Rongione, K. Conkrite, D. MacPherson

**Administrative, technical, or material support (i.e., reporting or organizing data, constructing databases):** M. Cui, M. Rongione, K. Conkrite, S. Parazzoli

**Study supervision:** D. MacPherson

### Acknowledgments

The authors thank Alison Pinder for performing next-generation sequencing, Sue Knoblauch for expert histopathology advice, and Tyler Jacks, Hong Wu, and Anton Berns for providing valuable mouse strains used in these studies.

### Grant Support

This work was supported by R01CA148867 (to D. MacPherson) and CA096823 (to A.Y. Nikitin).

The costs of publication of this article were defrayed in part by the payment of page charges. This article must therefore be hereby marked advertisement in accordance with 18 U.S.C. Section 1734 solely to indicate this fact.

Received October 15, 2013; revised January 17, 2014; accepted January 17, 2014; published OnlineFirst January 30, 2014.

## References

- Johnson BE, Ihde DC, Makuch RW, Gazdar AF, Carney DN, Oie H, et al. *myc* family oncogene amplification in tumor cell lines established from small cell lung cancer patients and its relationship to clinical status and course. *J Clin Invest* 1987;79:1629–34.
- Jackman DM, Johnson BE. Small-cell lung cancer. *Lancet* 2005;366:1385–96.
- Forgacs E, Biesterveld EJ, Sekido Y, Fong K, Muneer S, Wistuba II, et al. Mutation analysis of the PTEN/MMAC1 gene in lung cancer. *Oncogene* 1998;17:1557–65.
- Yokomizo A, Tindall DJ, Drabkin H, Gemmill R, Franklin W, Yang P, et al. PTEN/MMAC1 mutations identified in small cell, but not in non-small cell lung cancers. *Oncogene* 1998;17:475–9.
- Shibata T, Kokubu A, Tsuta K, Hirohashi S. Oncogenic mutation of PIK3CA in small cell lung carcinoma: a potential therapeutic target pathway for chemotherapy-resistant lung cancer. *Cancer Lett* 2009;283:203–11.
- Peifer M, Fernandez-Cuesta L, Sos ML, George J, Seidel D, Kasper LH, et al. Integrative genome analyses identify key somatic driver mutations of small-cell lung cancer. *Nat Genet* 2012;44:1104–10.
- Rudin CM, Durinck S, Stawiski EW, Poirier JT, Modrusan Z, Shames DS, et al. Comprehensive genomic analysis identifies SOX2 as a frequently amplified gene in small-cell lung cancer. *Nat Genet* 2012;44:1111–6.
- Pleasant ED, Stephens PJ, O'Meara S, McBride DJ, Meynert A, Jones D, et al. A small-cell lung cancer genome with complex signatures of tobacco exposure. *Nature* 2010;463:184–90.
- Meuwissen R, Linn SC, Linnoila RI, Zevenhoven J, Mooi WJ, Berns A. Induction of small cell lung cancer by somatic inactivation of both Trp53 and Rb1 in a conditional mouse model. *Cancer Cell* 2003;4:181–9.
- Dooley AL, Winslow MM, Chiang DY, Banerji S, Stransky N, Dayton TL, et al. Nuclear factor I/B is an oncogene in small cell lung cancer. *Genes Dev* 2011;25:1470–5.
- Park KS, Martelotto LG, Peifer M, Sos ML, Karnezis AN, Mahjoub MR, et al. A crucial requirement for Hedgehog signaling in small cell lung cancer. *Nat Med* 2011;17:1504–8.
- Schaffer BE, Park KS, Yiu G, Conklin JF, Lin C, Burkhart DL, et al. Loss of p130 accelerates tumor development in a mouse model for human small-cell lung carcinoma. *Cancer Res* 2010;70:3877–83.
- DuPage M, Dooley AL, Jacks T. Conditional mouse lung cancer models using adenoviral or lentiviral delivery of Cre recombinase. *Nat Protoc* 2009;4:1064–72.
- Li H, Durbin R. Fast and accurate long-read alignment with Burrows-Wheeler transform. *Bioinformatics* 2010;26:589–95.
- Li H, Handsaker B, Wysoker A, Fennell T, Ruan J, Homer N, et al. The Sequence Alignment/Map format and SAMtools. *Bioinformatics* 2009;25:2078–9.
- Wang K, Li M, Hakonarson H. ANNOVAR: functional annotation of genetic variants from high-throughput sequencing data. *Nucleic Acids Res* 2010;38:e164.
- Kim SK, Su LK, Oh Y, Kemp BL, Hong WK, Mao L. Alterations of PTEN/MMAC1, a candidate tumor suppressor gene, and its homologue, PTH2, in small cell lung cancer cell lines. *Oncogene* 1998;16:89–93.
- Sequist LV, Waltman BA, Dias-Santagata D, Digumarthy S, Turke AB, Fidias P, et al. Genotypic and histological evolution of lung cancers acquiring resistance to EGFR inhibitors. *Sci Transl Med* 2011;3:75ra26.
- Sutherland KD, Proost N, Brouns I, Adriaensen D, Song JY, Berns A. Cell of origin of small cell lung cancer: inactivation of Trp53 and Rb1 in distinct cell types of adult mouse lung. *Cancer Cell* 2011;19:754–64.

# Molecular Cancer Research

## PTEN Is a Potent Suppressor of Small Cell Lung Cancer

Min Cui, Arnaud Augert, Michael Rongione, et al.

*Mol Cancer Res* 2014;12:654-659. Published OnlineFirst January 30, 2014.

**Updated version** Access the most recent version of this article at:  
doi:[10.1158/1541-7786.MCR-13-0554](https://doi.org/10.1158/1541-7786.MCR-13-0554)

**Supplementary Material** Access the most recent supplemental material at:  
<http://mcr.aacrjournals.org/content/suppl/2014/01/31/1541-7786.MCR-13-0554.DC1>

**Visual Overview** **A diagrammatic summary of the major findings and biological implications:**  
<http://mcr.aacrjournals.org/content/12/5/654/F1.large.jpg>

**Cited articles** This article cites 19 articles, 3 of which you can access for free at:  
<http://mcr.aacrjournals.org/content/12/5/654.full#ref-list-1>

**Citing articles** This article has been cited by 17 HighWire-hosted articles. Access the articles at:  
<http://mcr.aacrjournals.org/content/12/5/654.full#related-urls>

**E-mail alerts** [Sign up to receive free email-alerts](#) related to this article or journal.

**Reprints and Subscriptions** To order reprints of this article or to subscribe to the journal, contact the AACR Publications Department at [pubs@aacr.org](mailto:pubs@aacr.org).

**Permissions** To request permission to re-use all or part of this article, use this link  
<http://mcr.aacrjournals.org/content/12/5/654>.  
Click on "Request Permissions" which will take you to the Copyright Clearance Center's (CCC) Rightslink site.